Journal of Materials Chemistry

Cite this: J. Mater. Chem., 2012, 22, 13764

www.rsc.org/materials

PAPER

Gum arabic assisted exfoliation and fabrication of Ag–graphene-based hybrids†

Jinchen Fan, Zixing Shi,* Yu Ge, Jialiang Wang, Yan Wang and Jie Yin

Received 8th March 2012, Accepted 16th April 2012
DOI: 10.1039/c2jm31437a

Gum arabic (GA), a natural polymer, is extensively used in food, drug, confectionery and soft drinks processing. In this paper, we present a green and facile approach for preparing graphene–Ag nanohybrids assisted by GA. In brief, GA functionalized graphene sheets (GA-G) were prepared by directly exfoliating graphite flakes in gum arabic (GA) aqueous solution with sonication. The yield of graphene exfoliation was systemically studied by varying the initial graphite concentration, GA concentration and sonication time. Furthermore, the GA functionalized graphene sheets–Ag nanoparticle hybrids (Ag/GA-G) were fabricated by adding $AgNO_3$ aqueous solution into the GA-G water dispersion. The silver ions were directly reduced and immobilized on the surface of the GA-G nanosheets by GA. The Ag/GA-G hybrid materials can be used as suitable substrates of SERS for the detection of 4-aminothiophenol (4-ATP) at a detectable level of a concentration of 10^{-6} M in aqueous environments.

Introduction

Graphene, a single layer graphite sheet that consists of sp^2 carbon atoms covalently bonded in a honeycomb crystal lattice,[1,2] has attracted a great deal of attention due to its fascinating properties such as thermal conductivity, mechanical properties and good electronic transport properties. With their high surface areas and extremely good electron mobility, graphene nanosheets (GS) have been applied in a wide range of applications, including catalysts, field-effect transistors, sensors, field emitters and hydrogen storage media.[3–12] Recently, graphene-based composites as a novel class of hybrid materials have aroused extensive interest in combining the desirable properties of building blocks for synergistic and new applications.[13–17] In order to further optimize the properties and enhancing applications of GS, various nanoparticles have been successfully decorated on graphene, such as metal and metal oxide nanoparticles (NPs). In this regard, various metal NPs/GS hybrid materials with metal or metal oxide NPs distributed onto the surface of graphene have been fabricated by the assembly of graphene sheets in the presence of inorganic precursors or pre-synthesized nanoparticles.[18–27]

Among the different kinds of metal NPs, Ag NPs are of great importance because of their catalytic, electrical, antibacterial properties and surface-enhanced Raman spectroscopy (SERS). Therefore, due to the high surface area (~2600 m^2 g^{-1}), and unique physical and chemical properties of graphene, considerable effort has been made to synthesize Ag/graphene composite materials. However, the traditional methods of preparing Ag/graphene composites were all based on graphene oxide (GO) or reduced graphene oxide (RGO).[25–42] There are some drawbacks in the traditional method of preparing Ag/graphene composites. GO is an insulator rather than a semi-metal and is conceptually different from graphene. Although the functional groups of GO can be removed by reduction, large defect populations continue to disrupt the properties.[43,44] Furthermore, Ag NPs obtained by the reduction of silver nitrate with either hydrazine or sodium borohydride suffer from problems, including poor stability and reproducibility, due to aggregation. In addition, the preparation protocol is relatively complex and many of them used toxic materials.

Therefore, it is desirable to develop a simple, good and green approach for direct exfoliation and reduction for preparing Ag/graphene composites. A significant breakthrough was made when the graphite could be exfoliated in certain solvents to high-throughput, giving defect-free graphene.[45,46] GS can be facilely obtained by the direct exfoliation of pristine graphite in certain liquid solutions, such as *N*-methyl-pyrrolidone (NMP), chlorosulfonic acid (CSA), methanesulfonic acid (MSA) and surfactant–water solutions.[40–46] However, among these liquid solutions, surfactant–water solutions exhibit promising developments due to

School of Chemistry & Chemical Technology, State Key Laboratory for Metal Matrix Composite Materials, Shanghai Jiao Tong University, Shanghai, 200240, China. E-mail: zxshi@sjtu.edu.cn; Fax: +86-21-54747445; Tel: +86-21-5474326

† Electronic supplementary information (ESI) available: 1. estimation of graphene concentration with the GA-stabilized aqueous graphene dispersions, 2. TEM and AFM images of GA-G nanosheets, 3. zeta potential (ζ) of graphite, GA, and GA-G aqueous dispersion, 4. the equilibrium contact angles of graphite and GA-G, 5. aqueous dispersibility of GA-G obtained with hot-air dry, 6. Raman spectroscopy of the reduced graphene oxide, and 7. TGA curves of Ag/GA-G hybrids. See DOI: 10.1039/c2jm31437a

their safety, biocompatibility and user-friendliness. Laaksonen *et al.* first demonstrated a one-step method for the exfoliation and functionalization of graphene by a surface-active protein. The Au/graphene hybrids were facilely obtained with the assistance of surface-active hydrophobin, which attaches to the graphene surface.[47] Amphipathic pyrene-labeled single stranded DNAs (Py-ssDNAs) were also used to fabricate Au/graphene nanocomposites through direct exfoliation and hybridization by Py-ssDNAs.[48] Based on this breakthrough, the fabrication of Ag/graphene hybrid materials directly by exfoliation and reduction in a surfactant–water solution could overcome the drawbacks of obtaining Ag/graphene nanocomposites from GO.

Gum arabic (GA), or gum acacia, is the oldest and best known of the tree gum exudates and can be obtained easily and abundantly.[49] It is extensively used in food, drugs, confectionery and soft drinks processing because it has an inherent ability to emulsify and stabilize flavouring oils dispersed in aqueous media.[49–53] Previous studies on the dispersion of carbon nanotubes (CNTs) showed that GA can serve as an effective dispersant to increase the dispersibility of CNTs in water.[54,55] Moreover, GA could act as a reducer, template and stabilizing agent for silver nanoparticles.[56–61]

Herein, we present a green and facile method to obtained Ag/graphene hybrids by GA. Water-dispersible GA functionalized graphene sheets (GA-G) were obtained by direct exfoliation from graphite flakes in the GA aqueous solution with sonication. The direct exfoliation results in a water-dispersible suspension of GA-coated flakes of graphene and ultrathin graphite. Then, the coated GA on the surface of graphene and ultrathin graphite was further used for the reduction and immobilization of Ag NPs to fabricate Ag/GA-G hybrids. Moreover, the Ag/GA-G hybrids can be used as an active SERS substrate for the detection of 4-aminothiophenol (4-ATP) in a liquid environment.

Experimental

Materials

Gum arabic (M_w = 220 000–300 000 Da) was purchased from Adamas Reagent Co., Ltd. Graphite powder (100 meshes, 99.9995%) and 4-aminothiophenol (4-ATP) were obtained from Alfa-Aesar Co. Ltd. Silver nitrate ($AgNO_3$) was supplied by Shanghai Chemical Reagent Co. All other reagents were at least of analytical reagent grade and were used without further purification.

Direct exfoliation and functionalization of graphene by gum arabic (GA)

Firstly, 2.0 g of GA was dissolved in 10 mL of water solution. Then, a set of natural graphite powders with different amounts were added into the gum arabic water solution under magnetic stirring for 1 h. After that, the graphite/GA water dispersion was sealed in the glass vials, followed by sonication for 6 h with an ultrasound bath cleaner at below 40 °C. After sonication, the dispersions were centrifuged at 4000 rpm for 30 min to sediment un-exfoliated particles or thick flakes of graphene, and GA-stabilized graphene aqueous dispersions were obtained by collecting the top supernatants. Successively, gum arabic functionalized graphene sheets (GA-G) were separated from the top supernatants by repeated centrifugation (15 000 rpm, 60 min) and with water washing steps. Finally, the GA-G was lyophilized in a freeze–dry system for 72 h to remove water completely.

Fabrication of Ag/GA-G hybrids and SERS experiments

A homogeneous GA-G aqueous dispersion (0.1 mg mL^{-1}) was prepared by adding 20 mg of GA-G into 200 mL of deionized water followed by sonication for 2 h. Then, 2 mL of $AgNO_3$ aqueous solution (2 mg mL^{-1}) was added into 1 mL of the above GA-G dispersion. Subsequently, the mixture solutions were allowed to stand undisturbed for different reaction times from 3 h to 6 h at 80 °C after being stirred for a few minutes. The weight ratios between the $AgNO_3$ and GA-G were varied from 240, 160, 80, to 40. Then, the Ag/GA-G hybrids were separated by centrifugation (15 000 rpm, 60 min) and washing with deionized (DI) water. The obtained Ag/GA-G hybrids were next redispersed into 5 mL of DI water for further use. For comparison, the GA-capped Ag NPs were prepared by adding 2 mL of the $AgNO_3$ aqueous solutions into 1 mL of pure GA aqueous solution (1 mg mL^{-1}) followed by the same procedure of obtaining Ag/GA-G hybrid materials.

Soaking was used to absorb the molecules on the surfaces of the Ag/GA-G hybrids. 0.5 mL of 4-aminothiophenol (4-ATP) aqueous solution with a concentration of 2×10^{-6} M was mixed with 0.5 mL of the as-prepared Ag/GA-G hybrids and GA-capped Ag NP colloids. After shaking, the mixture dispersions were allowed to stand for 3 h to reach the adsorption equilibrium for direct SERS detection in a liquid environment.

Characterization and instruments

The equilibrium contact angles were measured by a SL200B optical contact–angle meter (Kino industry, USA) at room temperature. UV-vis absorption spectra of the GA-stabilized graphene aqueous dispersion were recorded by a UV-2550 spectrophotometer (Shimadzu, Japan). Fourier transform infrared (FT-IR) spectra were recorded on a Perkin-Elmer Paragon 1000PC spectrometer. Transmission electron microscopy (TEM) images were obtained by a JEOL2100F. AFM images were recorded by a digital E-Sweep atomic force microscope in tapping mode. Raman spectra were taken with a Jobin Yvon micro-Raman spectroscope (RamLab-010), equipped with a holographic grating of 1800 lines per mm and a He–Ne laser (532 nm) as an excitation source. Thermogravimetric analysis (TGA) was performed with a Perkin-Elmer TGA 2050 instrument at a heating rate of 20 °C min^{-1}. X-Ray photoelectron (XPS) spectra were recorded on an ESCA LAB 250 spectrometer (VG Scientific) with Al Kα radiation (1486.6 eV). X-Ray powder diffraction (XRD) spectra were recorded on a D/max-2200/PC (Japan Rigaku Corp.) using CuKα radiation (λ = 1.5418 Å). The size distribution of the Ag NPs was measured by a Zetasizer Nano ZS90 instrument (Malvern Instruments) equipped with a 4 mW He–Ne laser (λ = 633 nm) at an angle of 90°, an avalanche photodiode detector with a high quantum efficiency, and an ALV/LSE-5003 multiple τ digital correlator electronics system.

Results and discussion

Direct exfoliation and functionalization of graphene by gum arabic

Graphene exfoliation was carried out by exposing a mixture of GA solution and graphite flakes to ultrasonic waves. By centrifuging at 4000 rpm for 30 min, the top supernatant, which was the final GA-stabilized graphene aqueous dispersion, was collected. As shown in Fig. 1, the obtained homogeneous GA-stabilized graphene aqueous dispersion was stable for long periods of time (over one month) in a sealed bottle.

This observation indicates that graphite is exfoliated with the presence of GA and a stable colloidal dispersion of graphene is achieved in the GA aqueous solution. The TEM images offer direct evidence for graphene exfoliation. Selected TEM images of graphene flakes were shown in Fig. 2. A small quantity of few-layer graphene flakes (<4 layers) was observed in Fig. 2a and b. The black dots in the TEM images are thought to be the GA coated on the surface of the graphene flakes. In Fig. 2c, there is a small graphene flake (~400 nm, 5 layers) stacked on a large flake (~0.8 μm) of 4 layers seen by paying close attention to the edges of flakes (Fig. 2d). The cross-sectional selected area electron diffraction (SAED) pattern, as shown in the inset of Fig. 2e, demonstrates the typical six-fold symmetry characteristic diffraction for graphene with an ordered, well-crystallized graphene structure. In some cases, the sheet edges of the graphene flakes tend to scroll and fold slightly (Fig. 2e). In addition, a large flake (~6 μm) was observed in Fig. 2f. It can be explained that the graphite was exfoliated to graphene flakes from the edge to the interlayers of the graphite. AFM images were also applied for investigating the topography and thickness of the GA-G nanosheets. The representative AFM images are shown in Fig. 3. The height profile in Fig. 3 shows a thickness of around 1.7–2.1 nm. Considering the GA which is coated on the surface of GS and the intrinsic limits of AFM,[62] the obtained graphene consists of less than 4 layers.

Lowering the high surface tension between the solution and the surface of graphite has been shown to facilitate the exfoliation of graphene. This proposal was supported by the investigation of the surface energy of graphene in the presence of GA by examining the wetting properties. Thus, the change in contact angle gives us guidelines as to the effect of GA on the wetting of graphene. Since graphite is known to be hydrophobic, the equilibrium contact angle was decreased from 110.3 to 73.3° after exfoliation by GA (Fig. S3, ESI†). This was expected since graphite is known to be hydrophobic. After exfoliation, the equilibrium contact angle for the GA-coated graphene flakes was 73.3°, indicating that the surface had turned hydrophilic. Amphiphilic gum arabic forms a layer where both of the sides have significantly different surface energies. Therefore, the mixing enthalpy of the graphene flakes coated with GA can be expressed in terms of the surface-energy differences among graphene, the hydrophobic polypeptide chains of GA, and the hydrophilic carbohydrate blocks.[63–65] The surface tension of water can be obviously reduced by GA due to significant surface activity.[66–68]

The yield of graphene exfoliation was studied by varying the initial graphite concentration, the GA concentration and the sonication time. In order to get the concentration of the GA-stabilized aqueous graphene dispersions after

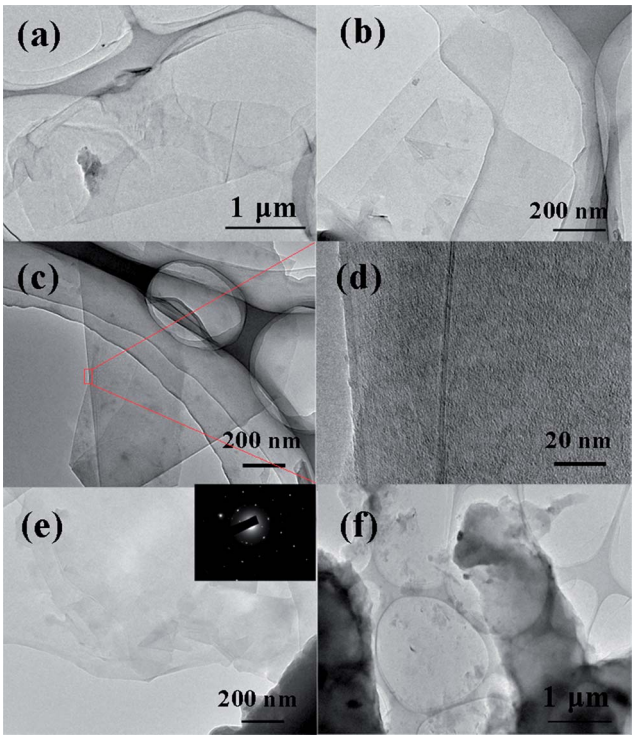

Fig. 2 Selected low-magnification TEM images of graphene flakes. (a),(b): typical TEM images of graphene flakes (<4 layers); (c): a small graphene flake stacked on a large graphene flake; (d): edge-on view of (c) at a higher magnification; (e): a large number of few-layer graphene flakes, inset of (e) shows a selected area electron diffraction (SAED) pattern; and (f): a large graphene flake with part exfoliation.

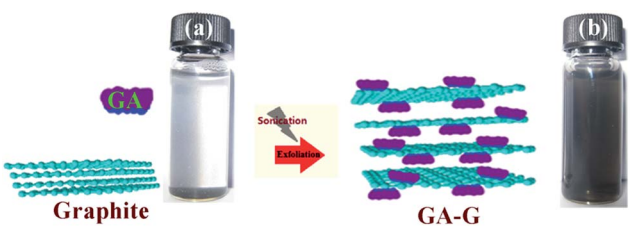

Fig. 1 Simple model for illustrating the process of graphene exfoliation (a) graphite/gum arabic (GA) initial aqueous dispersion, (b) GA-stabilized graphene aqueous dispersion.

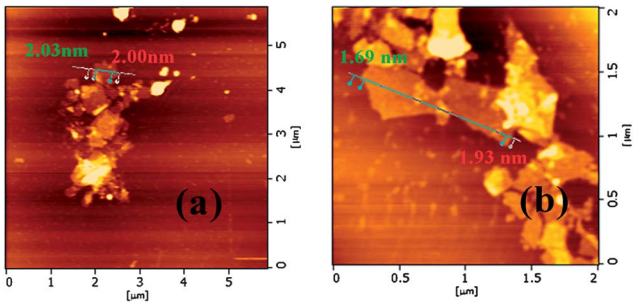

Fig. 3 AFM images of GA-G nanosheets deposited on mica substrates.

centrifugation, the obtained dispersions were diluted a number of times and the absorption spectra were recorded by UV-Vis-NIR. The spectra were measured in the 200–700 nm wavelength range. However, the absorption of GA approached zero at 500 nm and above (Fig. 11). Such observations allowed the use of the absorbance of the GA-stabilized aqueous graphene dispersions at 660 nm as a measure of the concentration of graphene. Therefore, the concentration was estimated from the absorbance at 660 nm by using the extinction coefficient of graphene (α = 1390 mL mg^{-1} m^{-1}), previously determined in surfactant–water solutions.[45,47–52] Using α for the graphene dispersion, the concentration of graphene nanosheets (C_{GS}) for the GA-stabilized aqueous graphene dispersions can be determined by the formula of the Lambert–Beer law (see ESI†). The efficiency of graphene exfoliation was investigated by varying the influence factors, including the initial concentration of graphite, the concentration of GA aqueous solution and the ultrasonication time. For measurement, 1.0 mL of the samples of the GA-stabilized aqueous graphene dispersions after centrifugation was diluted to 50 mL. The observed concentration of graphene for the GA-stabilized aqueous graphene dispersions is significantly affected by the initial concentration of graphite and GA. As shown in Fig. 4a, holding the concentration of GA constant at 130 mg mL^{-1}, the highest concentration of graphene achieved was 0.51 mg mL^{-1} with the initial concentration of graphite of 140 mg mL^{-1}. Then, the graphite concentration was fixed and the concentration of GA (C_{GA}) was varied. When C_{GA} reaches 100 mg mL^{-1}, the highest concentration of graphene obtained was 0.54 mg mL^{-1} (Fig. 4b). With regards to graphene exfoliation with surfactant, the yield of graphene is very close to the critical micelle concentration (CMC) of the surfactant.[62,71] When the concentration of GA exceeds 100 mg mL^{-1}, the C_{GS} exhibits an evident reduction. This is attributed to the high concentration of GA which is outside of the critical micelle concentration (CMC).[66,69,70] The effect of extending the sonication time up to several hours on the final concentration of the dispersed graphene was also monitored by measuring the absorbance of the suspensions at 660 nm. From Fig. 4c, the C_{GS} was increased with increasing sonication time. After sonication for 8 h, the C_{GS} can be up to 0.69 mg mL^{-1} with an initial graphite concentration of 140 mg mL^{-1} and a GA concentration of 100 mg mL^{-1}. To further understand the state of exfoliation, we performed a statistical analysis of the lateral dimensions and thickness of the GA-G nanosheets obtained by direct exfoliation with an initial graphite concentration of 140 mg mL^{-1} and a GA concentration of 100 mg mL^{-1} for 8 h sonication. The lateral distribution and thickness of the GA-G dimensions were calculated from a number of TEM and AFM images of 80 distinguishable GA-G nanosheets. These data are illustrated in the histogram for the standard dispersion in Fig. 5. The distributions of the lateral dimensions and the thickness were mainly concentrated in the range of 0.5–2 μm^2 and 2–6 nm, respectively. This demonstrated that graphene and ultrathin graphite of good quality can be facilely prepared by direct exfoliation with the assistance of GA.

In the process of preparing GA-stabilized aqueous graphene dispersions, GA also acted as the stabilizing and dispersing agent. Even though GA-G was obtained with hot-air drying at 80 °C, it has favourable dispersibility in water as well (Fig. S4, ESI†). The electrical properties of the obtained GA-G film were characterized by a four-point probe measurement. The GA-G films for the measurement were prepared by filtration of the resulting GA-G aqueous dispersion through a PTFE membrane filter (47 mm in diameter, 0.22 μm pore size), followed by extensive washing with water and peeling from the filter after air drying. The average DC conductivity of the GA-G films is ~787 S m^{-1}. This value is lower than that previously measured for similar films prepared from *N*-methyl-pyrrolidone-based dispersions (~6500 S m^{-1}).[71] This relative low DC conductivity is

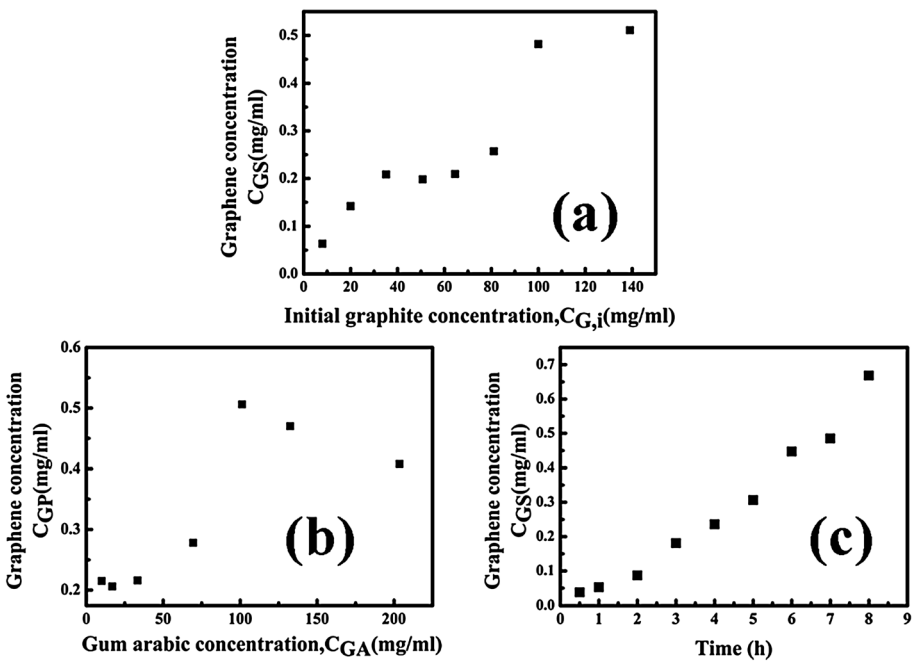

Fig. 4 Effects of (a) initial graphene concentration, (b) GA concentration, and (c) sonication time on the yield of graphene exfoliation.

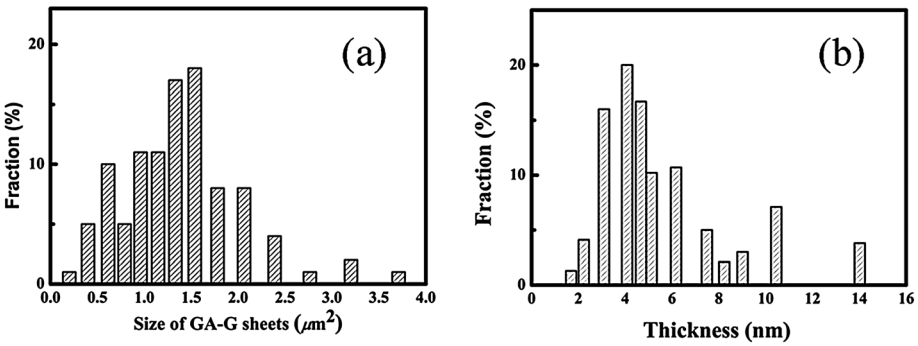

Fig. 5 The lateral dimensions (a) and thickness (b) of the GA-G nanosheets obtained by direct exfoliation with the assistance of GA.

mainly attributed to the GA coated on the surface of GS, which hampers the electrical conducting path in the film.[63]

The exfoliation of graphite into graphene was further demonstrated by Raman spectroscopy (Fig. 6). The pristine graphite is dominated by the G band (1576 cm^{-1}). There are two additional bands, D and D′ bands, located at 1324 and 1612 cm^{-1}, respectively.[70] After exfoliation, the D-band with a relatively strong intensity in the Raman spectroscopy of GA-G can be mainly ascribed to the increased fraction of graphene edges. The intensity ratio of the D and G band (I_D/I_G) reflects the structural defects and the indication of disorder. The I_D/I_G ratio increased from 0.07 for graphite to 0.29 for GA-G. Compared with the reduced graphene oxide (Fig. S5†), the ratio for GA-G is still quite low and this result indicates that GA-G contains low levels of defects.[71,72] The 2D band originates from second order double resonant Raman scattering from the zone boundary. It reflects the number of layers in the graphene samples, and can be used to distinguish single-layer, few-layer and multi-layer flakes. With the layers >5, the 2D-band of the graphene flakes strongly resembles the 2D-band for pristine graphite.[72,73] For the 2D band of GA-G, we noted that the width and shape are distinguished from pristine graphite. Therefore, we considered that the graphene and ultrathin graphite flakes can be obtained by direct exfoliation in the GA aqueous solution with sonication. This result is consistent with the TEM and AFM measurements.

Using the method of liquid exfoliation with GA, a water-dispersible suspension of GA-coated flakes of graphene and ultrathin graphite was obtained. The GA-G nanosheets were separated from the GA-stabilized graphene aqueous solution by repeating thirty cycles of centrifugation and with water washing steps for removing the excess GA. TGA, FT-IR and XPS measurements were also used to demonstrate the introduction of GA, which attaches to the surface of GS. The amount of GA in GA-G was determined by TGA (Fig. 7). Graphite shows an evident degradation at temperatures higher than 700 °C in an air atmosphere.[74] Judging from the weight loss which occurred at the plateau region around 800 °C, the amount of GA in the GA-G nanosheets was estimated to be approximately 56 wt%.

GA is a kind of non-ionic surfactant with a structure made up of a number of hydrophilic carbohydrate blocks (polysaccharide units) linked to hydrophobic polypeptide chains. FT-IR was also used to characterize the GA-G. From Fig. 8, the peaks at 1630 cm^{-1} and 1070 cm^{-1} in the spectra of GA-G are attributed to stretching vibrations of the C=O and C–O–C structures in the GA, respectively. Additional evidence that GA is present on the surface of graphene in the hybrid was obtained using X-ray photoelectron spectroscopy. As shown in Fig. 9, it is found that two new elements involving nitrogen and oxygen appear after exfoliation. While bulk graphite show a single carbon 1s XPS peak at 284.6 eV due to the presence of sp^2 C=C bonds, the XPS of the GA-G hybrid contains an O 1s peak at 531.9 eV, and a new weak N 1s peak at 399.8 eV, in addition to the C 1s peak. In addition, other new signals were clearly observed at *ca.* 287.5 eV (C=O), *ca.* 286.4 eV (C–O), *ca.* 285.8 eV (C–N), 285.2 eV (C–C) and 284.6 eV (C=C) (Fig. 9).[48,75]

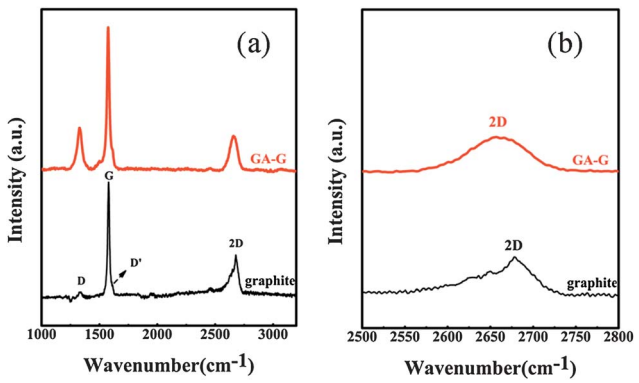

Fig. 6 (a) Raman spectroscopy of graphite and GA-G, (b) detailed 2D Raman band for GA-G and graphite.

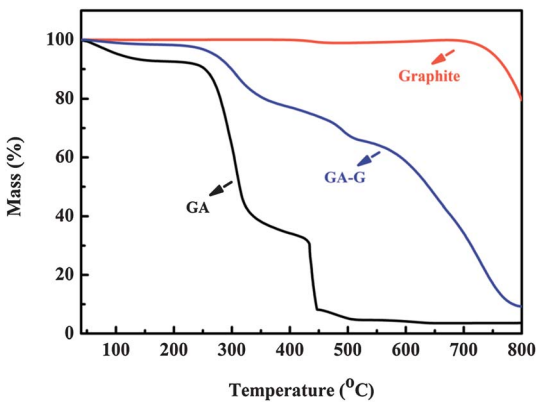

Fig. 7 TGA curves of graphite, GA and GA-G.

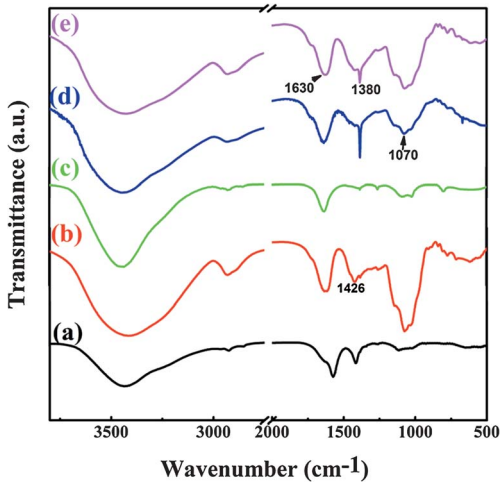

Fig. 8 FT-IR of (a) graphite, (b) GA, (c) GA-G, (d) GA-capped Ag NPs, and (e) Ag/GA-G hybrids.

Fabrication of Ag/GA-G hybrids and SERS experiments

It is well-known that the hydroxyl groups of polysaccharides can reduce silver metal to silver NPs through an oxidation mechanism. Upon the addition of silver nitrate aqueous solution to GA water solution, we have observed a change in the color of the mixture from transparent white (Fig. 10a) to yellow–brown (Fig. 10c) after standing at 80 °C for 3 h in room temperature. This color change is a direct and basic indication of the formation of Ag NPs, during which the ion-exchange process occurs, and the glycoprotein carboxylate groups (–COOH) of GA are converted into –COOAg. In a later stage, these silver ions, attached to the carboxylate groups, are converted into silver nanoparticles in an *in situ* manner.[58] In the FT-IR spectra of the GA-capped Ag NPs and Ag/GA-G, the transformations of the peak shape at 1380 cm^{-1} and 1426 cm^{-1} are attributed to the attachment of –COOH groups onto the silver NPs. With the direct exfoliation of graphene by GA, the structure of GA-G with GA coated on the surface of the graphene sheets can be used to reduce and immobilize the Ag NPs. For fabricating the Ag/GA-G hybrids, the aqueous dispersion of silver nitrate and GA-G was kept at 80 °C for 3 h and 6 h. The Ag/GA-G hybrids were also separated by repeating ten cycles of centrifugation and

Fig. 10 Photographs of (a) $AgNO_3$ aqueous solution, (b) GA aqueous solution, (c) a mixture of $AgNO_3$ and GA solution after reduction of silver ions, (d) a mixture of $AgNO_3$ and GA-G aqueous dispersion after reduction of silver ions and (e) Ag/GA-G hybrids redispersed in water.

with water washing steps for removing the excess non-immobilized Ag NPs. As shown in the UV-vis spectra (Fig. 11), compared with GA-G, the appearance of a new absorption peak at 417 nm demonstrates the formation of Ag NPs due to surface plasmon resonance (SPR) of Ag NPs.[29] X-Ray diffraction (XRD) was also used to characterize the fabrication of the Ag/GA-G hybrid film (Fig. 12). The peaks at 16–24° are ascribed to the crystallization of GA. The diffraction peak at 26.2° is attributed to the (002) reflection of a hexagonal graphite structure. After exfoliation, the diffraction peak at 26.2° still exists in the GA-G film. It indicates that the GA-G nanosheets restacked

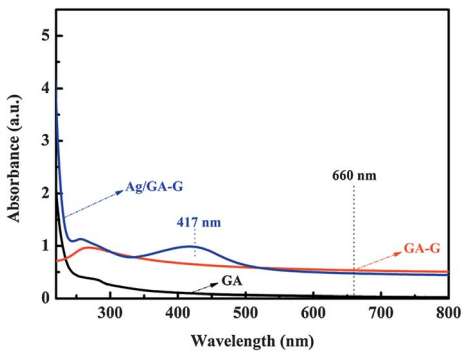

Fig. 11 The UV-vis absorption spectra of GA aqueous solution, GA-G aqueous dispersion, and Ag/GA-G hybrids redispersed in water.

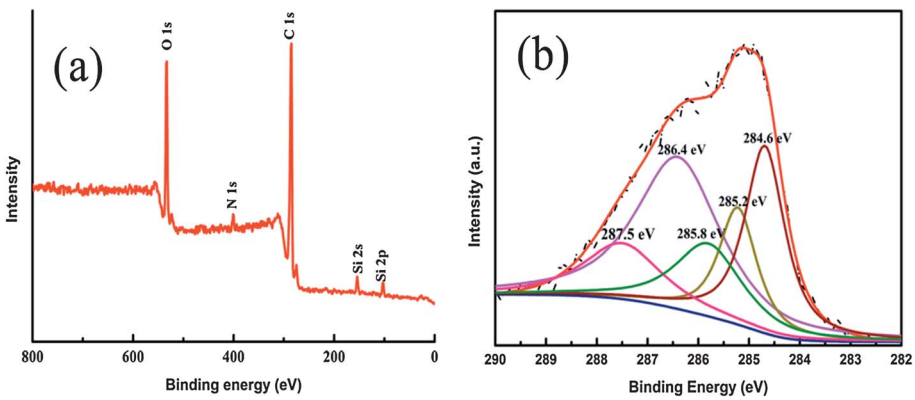

Fig. 9 XPS data for (a) GA-G and (b) core C 1s level.

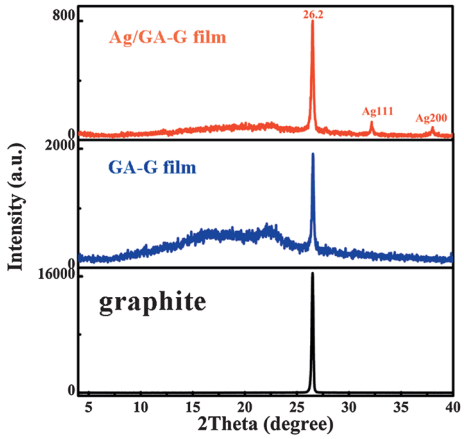

Fig. 12 XRD patterns of graphite, GA-G and Ag/GA-G hybrids.

to form a graphite-like structure in the film preparation process. It is worth noting that there is an evident decrease in the intensity value of the (002) diffraction peak from ~16 000 to ~2000. Meanwhile, the GA-G film shows no peak characteristic of graphene oxide at around 10°.[76,77] The results demonstrated the successful preparation of low defect graphene and ultrathin graphite flakes by direct exfoliation with the assistance of GA. The peak at (002) existed in the XRD patterns of the Ag/GA-G hybrids. The value of the intensity continued to decrease from ~2000 to ~800. This is because the attachment of Ag particles on the surface of the GA-G nanosheets prevents the stacking of graphene sheets.[78] The peaks at $2\theta = 32.3°$ and 38.2°, are assigned to the (111) and (200) crystalline planes of silver, respectively, which is attributed to the formation of Ag/GA-G hybrids with pure crystalline silver.[26] Furthermore, TEM images were conducted to characterize the Ag/GA-G hybrids. From Fig. 13a, b, d and e, the TEM images showed the Ag/GA-G hybrids with Ag NPs decorated on the surface of GA-G nanosheets. Therefore, we believe that Ag/GA-G hybrids with Ag NPs immobilized on the surface of GA-G nanosheets were successfully obtained with the assistance of GA.

Meanwhile, it is found that the size of the Ag NPs on the surface of the GA-G nanosheets can be controlled by changing the reaction time. Dynamic light scattering (DLS) also offers information about the size distribution of the Ag NPs with different reaction times. During the preparation of the Ag/GA-G hybrids, we collected the supernatant Ag NP colloid solution for DLS measurements during the separation and washing of Ag/GA-G. As shown in Fig. 13c and f, the average size of the Ag NPs increases from 6.4 nm to 9.6 nm with increasing reaction time. From Fig. 13d and e, after reaction for 6 h, there are some aggregates of Ag NPs of large size. This may be attributed to the effects of electrostatic interactions.[79] Thus, the Ag/GA-G hybrids obtained by the reaction for 3 h at 80 °C were used for the subsequent application of SERS. In addition, the density of the Ag NPs on the surface of the GA-G nanosheets increases with increasing of the weight ratio between $AgNO_3$ and GA-G. TGA analysis of the Ag/GA-G hybrids with different weight ratios between the $AgNO_3$ and GA-G illustrates that the Ag NP content of the Ag/GA-G increases from 35.87% to 70.96% with increasing weight ratio of $AgNO_3$ and GA-G (Fig. S6, ESI†).

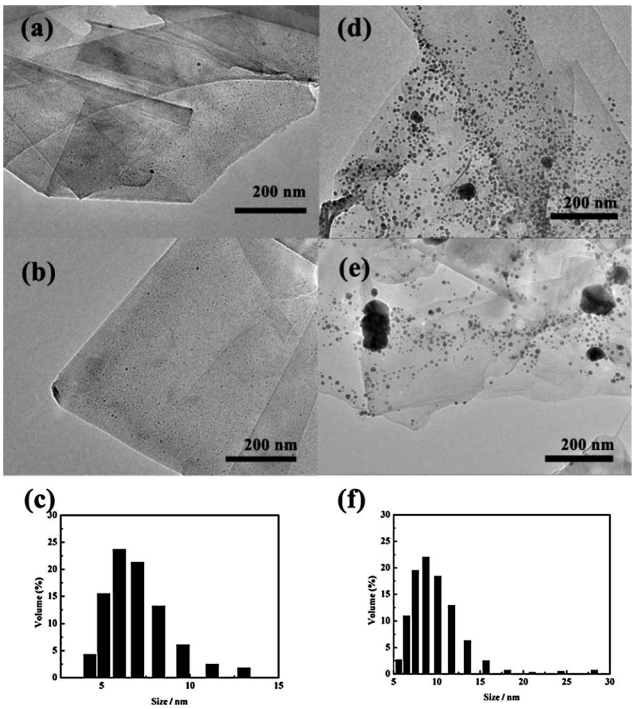

Fig. 13 (a and b): TEM images of Ag/GA-G nanohybrids with a reaction time of 3 h (size of Ag NPs: 5.1 ± 1.3 nm); (c): size distribution of Ag NPs with a reaction time of 3 h; (d and e): TEM images of Ag/GA-G nanohybrids with a reaction time of 6 h (size of Ag NPs: 10.7 ± 2.1 nm); (f): size distribution of Ag NPs with a reaction time of 6 h.

It is well-known that SERS is primarily due to highly concentrated electromagnetic (EM) fields. The hot spots of EM are often associated with interstitial sites in nanostructures, consisting of two or more coupled nanoparticles or otherwise nanostructured surfaces with closely spaced features.[80] To evaluate the SERS activity of the Ag/GA-G hybrids, 4-aminothiophenol (4-ATP) was used as a Raman probe molecule. As shown in Fig. 14, there is no evident Raman peak of 4-ATP detected on the surface of pure GA-G. Compared with the spectrum of the solid 4-ATP, there are distinct frequency shifts due to the changes in the band intensity. The deformation vibration of the carbon–sulfur (C–S) bond shift from 1092 to

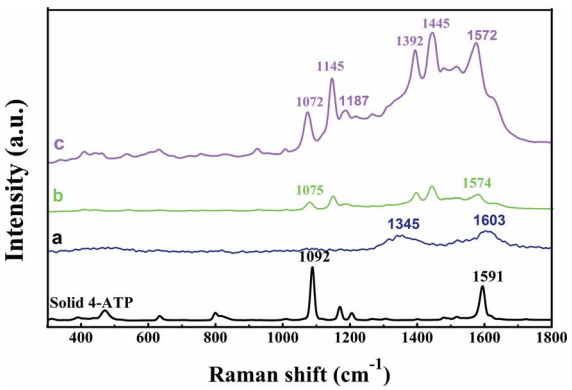

Fig. 14 Raman spectrum of solid 4-ATP, SERS spectra of 4-ATP (10^{-6} M) on (a) GA-G, (b) GA-capped Ag NPs, and (c) Ag/GA-G hybrids.

1074 cm^{-1}, and another frequency shift from 1591 to 1574 cm^{-1} were also observed. This is attributed to the formation of strong Ag–S bonds between the Ag NPs and –SH groups of 4-ATP.[81,82]

The SERS spectrum of 4-ATP on the Ag/GA-G hybrids exhibited four b_2 modes at 1145, 1392, 1445, and 1572 cm^{-1} and one a_1 mode at 1072 cm^{-1}. It is obvious that the intensity of the five bands in the SERS spectrum of 4-ATP on the Ag/GA-G hybrids was enlarged significantly. This indicates that the Ag/GA-G hybrids are suitable for the SERS of 4-ATP to reach a detectable level at a concentration of 10^{-6} M since the Ag NPs were immobilized on the surface of the GA-G sheets as hot spots for the strongly localized EM fields produced by the gaps between neighbouring Ag NPs.[80] Furthermore, the intensity of the SERS spectrum increased with increases of the weight ratio between $AgNO_3$ and GA-G (Fig. 15). This may be attributed to the increasing density of Ag NPs on the surface of the GA-G nanosheets. It is well known that 4-ATP molecules absorbed on the surface of the Ag/GA-G nanosheets were illuminated by laser light to obtain the corresponding SERS spectrum.[42] With the increasing amount of Ag NPs decorated on the surface of the GA-G nanosheets, the number of 4-ATP molecules absorbed on the surface of Ag/GA-G nanosheets per unit area increased.

Conclusions

In summary, we reported a facile and green method for obtaining Ag/GA-G hybrids with the assistance of GA. GA-functionalized graphene nanosheets were obtained by direct aqueous phase exfoliation in the presence of GA. The yields of graphene exfoliation were affected by the initial graphite concentration, GA concentration and the sonication time. Afterwards, Ag/GA-G hybrids with Ag NPs decorated on the graphene surface were prepared using GA as a reductant and stabilizer. The size and densities of the Ag NPs attached on the surface of the GA-G nanosheets can be adjusted by changing the reaction time and the weight ratio between $AgNO_3$ and GA-G. It is shown that the Ag/GA-G hybrids can be used as substrates for SERS for the detection of 4-ATP at a detectable level with a concentration of 10^{-6} M in a liquid environment. We believe that the approach for preparing the Ag/GA-G hybrids may have many further applications in biomaterials, biosensors, catalysis, *etc.*

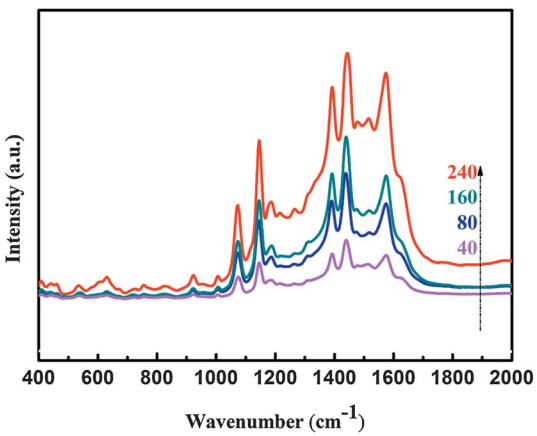

Fig. 15 SERS spectra of 4-ATP (10^{-6} M) on Ag/GA-G hybrids obtained with different weight ratios of $AgNO_3$ and GA-G: 40, 80, 160, and 240.

Acknowledgements

We thank the National Nature Science Foundation of China (no. 50973062) for the support. Additionally, we also acknowledge the staff of the Instrumental Analysis Center of Shanghai Jiao-Tong University for the measurements.

Notes and references

1 K. S. Novoselov, A. K. Geim, S. V. Morozov, D. Jiang, Y. Zhang, S. V. Dubonos, I. V. Grigorieva and A. A. Firsov, *Science*, 2004, **306**, 666–669.
2 K. S. Novoselov, A. K. Geim, S. V. Morozov, D. Jiang, M. I. Katsnelson, I. V. Grigorieva, S. V. Dubonos and A. A. Firsov, *Nature*, 2005, **438**, 197–200.
3 S. Stankovich, D. A. Dikin, G. H. B. Dommett, K. M. Kohlhaas, E. J. Zimney, E. A. Stach, R. D. Piner, S. T. Nguyen and R. S. Ruoff, *Nature*, 2006, **442**, 282–286.
4 J. T. Robinson, F. K. Perkins, E. S. Snow, Z. Wei and P. E. Sheehan, *Nano Lett.*, 2008, **8**, 3137–3140.
5 J. D. Fowler, M. J. Allen, V. C. Tung, Y. Yang, R. B. Kaner and B. H. Weiller, *ACS Nano*, 2009, **3**, 301–306.
6 S. De, P. J. King, M. Lotya, A. O'Neill, E. M. Doherty, Y. Hernandez, G. S. Duesberg and J. N. Coleman, *Small*, 2010, **6**, 458–464.
7 X. Li, Y. Zhu, W. Cai, M. Borysiak, B. Han, D. Chen, R. D. Piner, L. Colombo and R. S. Ruoff, *Nano Lett.*, 2009, **9**, 4359–4363.
8 C. Liu, Z. Yu, D. Neff, A. Zhamu and B. Z. Jang, *Nano Lett.*, 2010, **10**, 4863–4868.
9 G. Wang, X. Shen, J. Yao and J. Park, *Carbon*, 2009, **47**, 2049–2053.
10 L. L. Zhang, R. Zhou and X. S. Zhao, *J. Mater. Chem.*, 2010, **20**, 5983–5992.
11 M. H. Liang and L. J. Zhi, *J. Mater. Chem.*, 2009, **19**, 5871–5878.
12 V. Eswaraiah, K. Balasubramaniam and S. Ramaprabhu, *J. Mater. Chem.*, 2011, **21**, 12626–12628.
13 C. Yuan, W. Chen and L. Yan, *J. Mater. Chem.*, 2012, **22**, 7456–7460.
14 H. Y. Koo, H.-J. Lee, Y.-Y. Noh, E.-S. Lee, Y.-H. Kim and W. S. Choi, *J. Mater. Chem.*, 2012, **22**, 7130–7135.
15 H. Lee, J. Kang, M. S. Cho, J.-B. Choi and Y. Lee, *J. Mater. Chem.*, 2011, **21**, 18215–18219.
16 Y. Wang, H.-B. Yao, X.-H. Wang and S.-H. Yu, *J. Mater. Chem.*, 2011, **21**, 562–566.
17 Z. Luo, L. Yuwen, B. Bao, J. Tian, X. Zhu, L. Weng and L. Wang, *J. Mater. Chem.*, 2012, **22**, 7791–7796.
18 J. Ji, G. Zhang, H. Chen, Y. Li, G. Zhang, F. Zhang and X. Fan, *J. Mater. Chem.*, 2011, **21**, 14498–14501.
19 P. V. Kamat, *J. Phys. Chem. Lett.*, 2010, **1**, 520–527.
20 H. F. Shi, Z. S. Li, J. H. Kou, J. H. Ye and Z. G. Zou, *J. Phys. Chem. C*, 2011, **115**, 145–151.
21 C. Xu, X. Wang, J. W. Zhu, X. J. Yang and L. Lu, *J. Mater. Chem.*, 2008, **18**, 5625–5629.
22 J. F. Shen, M. Shi, N. Li, B. Yan, H. W. Ma, Y. Z. Hu and M. X. Ye, *Nano Res.*, 2010, **3**, 339–349.
23 B. Li, G. Lu, X. Z. Zhou, X. H. Cao, F. Boey and H. Zhang, *Langmuir*, 2009, **25**, 10455–10458.
24 C. Xu, X. Wang and J. W. Zhu, *J. Phys. Chem. C*, 2008, **112**, 19841–19845.
25 J. F. Shen, M. Shi, B. Yan, H. W. Ma, N. Li and M. X. Ye, *J. Mater. Chem.*, 2011, **21**, 7795–7801.
26 W. P. Xu, L. C. Zhang, J. P. Li, Y. Lu, H. H. Li, Y. N. Ma, W. D. Wang and S. H. Yu, *J. Mater. Chem.*, 2011, **21**, 4593–4597.
27 S. S. J. Aravind, V. Eswaraiah and S. Ramaprabhu, *J. Mater. Chem.*, 2011, **21**, 17094.
28 Z. Zhang, F. G. Xu, W. S. Yang, M. Y. Guo, X. D. Wang, B. L. Zhanga and J. L. Tang, *Chem. Commun.*, 2011, **47**, 6440–6442.
29 R. Pasricha, S. Gupta and A. K. Srivastava, *Small*, 2009, **5**, 2253–2259.
30 J. Li and C. Y. Liu, *Eur. J. Inorg. Chem.*, 2010, 1244–1248.
31 S. Liu, L. Wang, J. Q. Tian, Y. L. Luo, X. X. Zhang and X. P. Sun, *J. Colloid Interface Sci.*, 2011, **363**, 615–619.
32 Z. X. Xu, H. Y. Gao and H. Guoxin, *Carbon*, 2011, **49**, 4731–4738.
33 Y. Wan, Y. Wang, J. J. Wu and D. Zhag, *Anal. Chem.*, 2011, **83**, 648–653.

34 G. Lu, H. Li, C. Liusman, Z. Y. Yin, S. X. Wu and H. Zhang, *Chem. Sci.*, 2011, **2**, 1817–1821.
35 S. Liu, J. Q. Tian, L. Wang and X. P. Sun, *J. Nanopart. Res.*, 2011, **13**, 4539–4548.
36 T. T. Baby and S. Ramaprabhu, *J. Mater. Chem.*, 2011, **21**, 9702–9709.
37 S. Liu, J. Q. Tian, L. Wang and X. P. Sun, *Carbon*, 2011, **49**, 3158–3164.
38 E. C. Ou, X. J. Zhang, Z. M. Chen, Y. G. Zhan, Y. Du, G. P. Zhang, Y. J. Xiang, Y. Q. Xiong and W. J. Xu, *Chem.–Eur. J.*, 2011, **17**, 8789–8793.
39 W. Ren, Y. X. Fang and E. K. Wang, *ACS Nano*, 2011, **5**, 6425–6433.
40 T. S. Wu, S. Liu, Y. L. Luo, W. B. Lu, L. Wang and X. P. Sun, *Nanoscale*, 2011, **3**, 2142–2144.
41 Y. K. Yang, C. E. He, W. J. He, L. J. Yu, R. G. Peng, X. L. Xie, X. B. Wang and Y. W. Mai, *J. Nanopart. Res.*, 2011, **13**, 5571–5581.
42 Z. Zhang, F. Xu, W. Yang, M. Guo, X. Wang, B. Zhang and J. Tang, *Chem. Commun.*, 2011, **47**, 6440–6442.
43 D. R. Dreyer, S. Park, C. W. Bielawski and R. S. Ruoff, *Chem. Soc. Rev.*, 2010, **39**, 228–240.
44 S. Watcharotone, D. A. Dikin, S. Stankovich, R. Piner, I. Jung, G. H. B. Dommett, G. Evmenenko, S. E. Wu, S. F. Chen, C. P. Liu, S. T. Nguyen and R. S. Ruoff, *Nano Lett.*, 2007, **7**, 1888–1892.
45 M. Lotya, Y. Hernandez, P. J. King, R. J. Smith, V. Nicolosi, L. S. Karlsson, F. M. Blighe, S. De, Z. Wang, I. T. McGovern, G. S. Duesberg and J. N. Coleman, *J. Am. Chem. Soc.*, 2009, **131**, 3611–3620.
46 N. G. Shang, P. Papakonstantinou, S. Sharma, G. Lubarsky, M. Li, D. W. McNeill, A. J. Quinn, W. Zhou and R. Blackley, *Chem. Commun.*, 2012, **48**, 1877–1879.
47 P. Laaksonen, M. Kainlauri, T. Laaksonen, A. Shchepetov, H. Jiang, J. Ahopelto and M. B. Linder, *Angew. Chem., Int. Ed.*, 2010, **49**, 4946–4949.
48 F. Liu, J. Y. Choi and T. S. Seo, *Chem. Commun.*, 2010, **46**, 2844–2846.
49 M. Nakauma, T. Funami, S. Noda, S. Ishihara, S. Al-Assaf, K. Nishinari and G. O. Phillips, *Food Hydrocolloids*, 2008, **22**, 1254–1267.
50 S. Krishnan, A. C. Kshirsagar and R. S. Singhal, *Carbohydr. Polym.*, 2005, **62**, 309–315.
51 F. M. Ward, *Cell and Developmental Biology of Arabinogalactan-Proteins*, 2000, pp. 231–239.
52 B. Wang, L. J. Wang, D. Li, B. Adhikari and J. Shi, *Carbohydr. Polym.*, 2011, **86**, 343–351.
53 D. Djordjevic, L. Cercaci, J. Alamed, D. J. McClements and E. A. Decker, *Food Chem.*, 2008, **106**, 698–705.
54 R. Bandyopadhyaya, E. Nativ-Roth, O. Regev and R. Yerushalmi-Rozen, *Nano Lett.*, 2002, **2**, 25–28.
55 V. Datsyuk, P. Landois, J. Fitremann, A. Peigney, A. M. Galibert, B. Soula and E. Flahaut, *J. Mater. Chem.*, 2009, **19**, 2729–2736.
56 A. C. A. Roque, A. Bicho, I. L. Batalha, A. S. Cardoso and A. Hussain, *J. Biotechnol.*, 2009, **144**, 313–320.
57 V. Kattumuri, K. Katti, S. Bhaskaran, E. J. Boote, S. W. Casteel, G. M. Fent, D. J. Robertson, M. Chandrasekhar, R. Kannan and K. V. Katti, *Small*, 2007, **3**, 333–341.
58 Y. M. Mohan, K. M. Raju, K. Sambasivudu, S. Singh and B. Sreedhar, *J. Appl. Polym. Sci.*, 2007, **106**, 3375–3381.
59 C. C. Wu and D. H. Chen, *Gold Bull.*, 2010, **43**, 234–240.
60 G. M. Fent, S. W. Casteel, D. Y. Kim, R. Kannan, K. Katti, N. Chanda and K. Katti, *Nanomed.: Nanotechnol., Biol. Med.*, 2009, **5**, 128–135.
61 P. Kan, H. P. Engelbrecht, L. D. Watkinson, T. L. Carmack, J. R. Lever, C. J. Smith, R. Kannan, K. V. Kattesh, S. S. Jurisson and C. S. Cutler, *J. Labelled Compd. Radiopharm.*, 2009, **52**, S521.
62 P. Lemoine, J. F. Zhao, A. Bell, P. Maguire and J. McLaughlin, *Diamond Relat. Mater.*, 2001, **10**, 94–98.
63 Y. Dror, Y. Cohen and R. Yerushalmi-Rozen, *J. Polym. Sci., Part B: Polym. Phys.*, 2006, **44**, 3265–3271.
64 B. H. Ali, A. Ziada and G. Blunden, *Food Chem. Toxicol.*, 2009, **47**, 1–8.
65 A. M. Islam, G. O. Phillips, A. Sljivo, M. J. Snowden and P. A. Williams, *Food Hydrocolloids*, 1997, **11**, 493–505.
66 E. Dickinson, B. S. Murray, G. Stainsby and D. M. W. Anderson, *Food Hydrocolloids*, 1988, **2**, 477–490.
67 N. Garti, Y. Slavin and A. Aserin, *Food Hydrocolloids*, 1999, **13**, 145–155.
68 N. Garti and D. Reichman, *Food Hydrocolloids*, 1994, **8**, 155–173.
69 C. Sanchez, D. Renard, P. Robert, C. Schmitt and J. Lefebvre, *Food Hydrocolloids*, 2002, **16**, 257–267.
70 M. Lotya, Y. Hernandez, P. J. King, R. J. Smith, V. Nicolosi, L. S. Karlsson, F. M. Blighe, S. De, Z. M. Wang, I. T. McGovern, G. S. Duesberg and J. N. Coleman, *J. Am. Chem. Soc.*, 2009, **131**, 3611–3620.
71 Y. Hernandez, V. Nicolosi, M. Lotya, F. M. Blighe, Z. Y. Sun, S. De, I. T. McGovern, B. Holland, M. Byrne, Y. K. Gun'ko, J. J. Boland, P. Niraj, G. Duesberg, S. Krishnamurthy, R. Goodhue, J. Hutchison, V. Scardaci, A. C. Ferrari and J. N. Coleman, *Nat. Nanotechnol.*, 2008, **3**, 563–568.
72 D. Graf, F. Molitor, K. Ensslin, C. Stampfer, A. Jungen, C. Hierold and L. Wirtz, *Nano Lett.*, 2007, **7**, 238–242.
73 I. Calizo, A. A. Balandin, W. Bao, F. Miao and C. N. Lau, *Nano Lett.*, 2007, **7**, 2645–2649.
74 E.-K. Choi, I.-Y. Jeon, S.-Y. Bae, H.-J. Lee, H. S. Shin, L. Dai and J.-B. Baek, *Chem. Commun.*, 2010, **46**, 6320–6322.
75 Y. Wang, Y. Y. Shao, D. W. Matson, J. H. Li and Y. H. Lin, *ACS Nano*, 2010, **4**, 1790–1798.
76 H. A. Becerril, J. Mao, Z. Liu, R. M. Stoltenberg, Z. Bao and Y. Chen, *ACS Nano*, 2008, **2**, 463–470.
77 W. Lu, S. Liu, X. Qin, L. Wang, J. Tian, Y. Luo, A. M. Asiri, A. O. Al-Youbi and X. Sun, *J. Mater. Chem.*, 2012, **22**, 8775–8777.
78 J. Yang, C. Zang, L. Sun, N. Zhao and X. Cheng, *Mater. Chem. Phys.*, 2011, **129**, 270–274.
79 A. M. E. Badawy, T. P. Luxton, R. G. Silva, K. G. Scheckel, M. T. Suidan and T. M. Tolaymat, *Environ. Sci. Technol.*, 2010, **44**, 1260–1266.
80 S. J. Lee, A. R. Morrill and M. Moskovits, *J. Am. Chem. Soc.*, 2006, **128**, 2200–2201.
81 R. G. Freeman, K. C. Grabar, K. J. Allison, R. M. Bright, J. A. Davis, A. P. Guthrie, M. B. Hommer, M. A. Jackson, P. C. Smith, D. G. Walter and M. J. Natan, *Science*, 1995, **267**, 1629–1632.
82 S. E. Hunyadi and C. J. Murphy, *J. Mater. Chem.*, 2006, **16**, 3929.

